Article

Interfacial Design of Mixed Matrix Membranes via Grafting PVA on UiO-66-NH$_2$ to Enhance the Gas Separation Performance

Saeed Ashtiani [1,*], Mehdi Khoshnamvand [2], Chhabilal Regmi [1] and Karel Friess [1,*]

[1] Department of Physical Chemistry, University of Chemistry and Technology, Prague, Technická 5, 16628 Prague 6, Czech Republic; regmic@vscht.cz

[2] State Key Laboratory of Environmental Chemistry and Ecotoxicology, Research Center for Eco-Environmental Sciences, Chinese Academy of Sciences, Beijing 100085, China; mehdi.khoshnam@yahoo.com

[*] Correspondence: jamalias@vscht.cz (S.A.); friessk@vscht.cz (K.F.)

Abstract: In this study, defect-free facilitated transport mixed matrix membrane (MMM) with high loading amount of UiO-66-NH$_2$ nanoparticles as metal–organic frameworks (MOFs) was fabricated. The MOFs were covalently bonded with poly (vinyl alcohol) (PVA) to incorporate into a poly (vinyl amine) (PVAm) matrix solution. A uniform UiO-66-NH$_2$ dispersion up to 55 wt.% was observed without precipitation and agglomeration after one month. This can be attributed to the high covalent interaction at interfaces of UiO-66-NH$_2$ and PVAm, which was provided by PVA as a functionalized organic linker. The CO$_2$ permeability and CO$_2$/N$_2$ and selectivity were significantly enhanced for the fabricated MMM by using optimal fabrication parameters. This improvement in gas performance is due to the strong impact of solubility and decreasing diffusion in obtained dense membrane to promote CO$_2$ transport with a bicarbonate reversible reaction. Therefore, the highest amount of amine functional groups of PVAm among all polymers, plus the abundant amount of amines from UiO-66-NH$_2$, facilitated the preferential CO$_2$ permeation through the bicarbonate reversible reaction between CO$_2$ and –NH$_2$ in humidified conditions. XRD and FTIR were employed to study the MMM chemical structure and polymers–MOF particle interactions. Cross-sectional and surface morphology of the MMM was observed by SEM-EDX and 3D optical profilometer to detect the dispersion of MOFs into the polymer matrix and explore their interfacial morphology. This approach can be extended for a variety of polymer–filler interfacial designs for gas separation applications.

Keywords: metal–organic framework; mixed-matrix membrane; interface engineering; UiO-66-NH$_2$

1. Introduction

It is generally accepted that CO$_2$ as a gas is known as the primary source of climate change and is required to be separated from flue gas to eliminate the greenhouse effect [1]. Thus far, various types of separation techniques such as adsorption, absorption [2], cryogenic distillation [3], microbial and algal have been applied for the protection of the global environment by CO$_2$ emission [4]. Although these conventional methods have been successfully employed for the separation of CO$_2$, some principal drawbacks such as the immense amount of adsorbents, low adsorbing surface area, high operational and maintenance cost, and equipment corrosion problems highlight the absence of effective worldwide technology for CO$_2$ separation [5,6]. Membrane-based separation processes offer a promising alternative for this purpose due to their compact design, cost-effectiveness, high surface area, ease of maintenance, and environmentally friendly nature [7]. Nevertheless, inorganic membranes possess high chemical and thermal stability with high selectivity. They are oxidized because of their low permeability due to the requirement of a thicker layer to prevent pinholes and cracks [8]. Polymeric membranes exhibit good permeability and easy processability but their low mechanical and thermal stability limit their wide

range of industrial applications. Therefore, organic and inorganic hybrid membranes take advantage of both polymeric and inorganic membranes to surpass the 2008 Robeson upper bound limit where the selectivity is plotted against the CO_2 permeability [9]. Generally, the Robeson plots and corresponding upper bounds are the benchmarks used to evaluate the membrane separation performance for various gas pairs. This type of plot can also judge the relative potential of new membrane materials for exceeding the upper bound line [10].

The most important challenges in the hybrid membrane are the strong interface interaction between the organic and the inorganic phases, and the uniform dispersion of the inorganic particles. Mixed matrix membranes (MMMs) represent a specific type of hybrid membrane forms with incorporated filler into the continuous polymer matrix. The embedded filler particles are commonly different inorganic materials with inherent superior separation characteristics such as nanoparticles, carbon molecular sieves, zeolites, etc. [11]. A metal–organic framework (MOF) is a crystalline-structured porous material, which is synthesized by the uniform arrangement of positively charged metal ions that interact with the organic linker or cluster molecules. The larger surface area, void volumes, pore connectivity, and chemical and thermal stability of the MOFs have drawn intense efforts compared to the other filler materials, especially for gas sorption and vapors [12]. As aforementioned, particle dispersion problems such as aggregation, sedimentation, and polymer–MOF interface morphology challenges such as weak adhesion between polymer and MOF, polymer chain rigidification, and MOFs pore blockage by the polymer chains, result in deterioration of gas separation performance of the MMM [13]. Therefore, obtaining a homogenous dispersion of MOFs into the polymer matrix to achieve a defect-free polymer–MOF interface and appropriate combination of polymer and MOFs are the key elements controlling the final separation performances of the MMM, which need to be addressed. Wu et al. [14], reported a dual-interfacial approach to engineering the MOF-74 to obtain a polycrystalline MOF-74 intermediate layer on the core MOF surface to divide the single MOF interface to the MOF–MOF and MOF–polymer interfaces. It resulted in the growth of the Ni-MOF-7 shell layer to prevent the gas molecules' transport horizontally, causing increment of C_2H_4/C_2H_6 selectivity. Moreover, to obtain effective separation performances in MMM, a good MOF configuration to maximize the polymer–MOF interaction is required, forcing the gas molecules to pass through the interconnected MOF channel and the polymer matrix. Recently, Hossain et al. [15] prepared cross-linked MMM by covalently anchoring the attaching polyethylene glycol (PEG)/polypropylene glycol (PPG)–polydimethylsiloxane (PDMS) to UiO-66 using ring-opening metathesis polymerization to improve the compatibility of MOF with the polymer matrix and prevent the MOF sedimentation during the casting process. Compared to other methods, it is particularly challenging to obtain the favorable MOF–polymer interface structure using the random blending method, as long as H-bonding or $\pi-\pi$ stacking is taking place instead of strong chemical bonds at the MOF–polymer interfaces. Furthermore, the mentioned methods, such as dual-interfacial approach [14], in situ polymerization [16], grafting-to, and grafting-from strategies [17], demand several complicated modification steps, high fabrication cost, and are limited by facilities, as they can be applied in lab-scale processes from a fundamental point of view.

Recently, our group developed a simple and effective approach using the "bridging technique" [18] to strengthen the interfacial interactions of MOF–polymer for pushing the 2008 Robeson upper bound limit. In this method, opposed to the methods above, the MOF particles were modified before incorporation into the polymer matrix, since the MMM molecular engineering of the MMM structure mainly takes place before the membrane casting process. This method benefits from the bridging technique and facilitated transport mechanisms [19], which hasten the preferential reactive gas adsorption such as CO_2 over non-reactive gas molecules diffusion such as H_2, N_2, and CH_4.

Therefore, in this work we developed our previous concept, by fabrication of a UiO-66-NH_2-PVA-PVAm facilitated transport mixed matrix membrane (FT-MMM), where PVA polymer chains were primarily grafted-onto the synthesized UiO-66-NH_2 followed by

embedding into the PVAm matrix. The UiO-66-NH$_2$ was chosen since it provided sufficient amount of –NH$_2$ groups for both providing CO$_2$ fixed-carrier sites, as well as PVAm, and also its high stability in aqueous media. This method grants a robust adhesion between PVAm and the UiO-66-NH$_2$ through the PVA polymer chains to the uniform dispersion of UiO-66 to form a defect-free MMM even up to 55 wt.% of MOF loading. The fabricated membranes were characterized using X-ray diffraction (XRD) analysis, Fourier-transform infrared spectroscopy (FTIR), and Raman spectroscopy measurements to evaluate the chemical interactions between the MMM components. Scanning electron microscopy (SEM) coupled with energy-dispersive X-ray spectroscopy (EDX), 3D optical profilometers were used to observe the obtained morphology and monitor the UiO-66-NH$_2$ dispersion into the PVAm matrix. The gas separation performances of the MMM were measured using a gas chromatograph (TR-TC6891 N) for the separation of CO$_2$/N$_2$ mixture gas at atmospheric pressure and room temperature. The effect of the UiO-66-NH$_2$-PVA loading amount on the gas separation performances of the MMMs was also investigated by using 0–55 wt.% of MOF–PVA amount. The overall physiochemical and gas separation properties of the fabricated MMM showed dramatic changes by enhancing MOF–polymer interface interactions using the bridging technique as an effective method to design desirable MMM defect-free morphology.

2. Materials and Methods

2.1. Materials

Commercial poly (vinyl amine) (PVAm) pellets (Lupamin-9095, Mw 340,000 g/mol) were obtained by BASF (Jakarta, Indonesia). Poly (vinyl alcohol) (PVA) (Mw: 31,000 g/mol) was provided by Sigma-Aldrich (St. Louis, MO, USA). Ethanol of 96% purity was purchased from Penta (Prague, Czech Republic). 2-Aminoterephthalic acid, zirconium chloride (ZrCl$_4$), hydrochloric acid (HCl), and dimethylformamide (DMF) with 96% purity for synthesizing MOF particles were obtained from Merck (Prague, Czech Republic). All the obtained chemicals were used as received without further purification.

2.2. Characterization

Fourier-transform infrared spectroscopy (FTIR) measurements were conducted on a Nicolet iS50 FTIR Spectrometer (Thermo Scientific, Waltham, MA, USA) to study the physicochemical interactions between the MMM components. The membrane sample was fixed onto the attenuated total reflection (ATR) diamond crystal surface, using a deuterated triglycine sulfate detector for measurements in the range of 500–4000 cm^{-1} for all samples. X-ray powder diffraction (XRD) was performed at room temperature using a Bruker D8 Discoverer θ-θ powder diffractometer (Karlsruhe, Germany) with para-focusing Bragg–Brentano geometry with CuKαradiation (λ = 0.15418 nm, U = 40 kV, I = 40 mA). Data were scanned at an angular range of 5–80° (2θ) to determine the crystal structure of MMM by incorporating different MOF loading amounts. The morphology of the fabricated MMM was investigated by scanning electron microscopy (SEM) (Oxford instruments, Tokyo, Japan). The 3D non-contact optical surface profiler NewView 9000 (ZYGO, Prague, Czech Republic) was used for precise, quantities, non-contact surface measurement and characterization.

2.3. Synthesis of UiO-66-NH$_2$

The UiO-66-NH$_2$ MOF particles were synthesized similar to previous reports [12,18]. In brief, 6.4 g of zirconium (IV) chloride (ZrCl$_4$) and 5 g of 2-aminoterephthalic acid were dissolved in 25 mL DMF separately for 1 h at room temperature. The solution was placed into a 100 mL Teflon-lined autoclave for proceeding with the solvothermal synthesis at 120 °C overnight while keeping the solution stagnant. The obtained yellow product was centrifuged for 15 min at 9000 rpm, and the precipitate was washed twice with DMF and methanol. The yellow particles were dried and activated in a vacuum oven at 150 °C for 24 h.

2.4. Fabrication of UiO-66-NH$_2$-PVA-PVAm Mixed Matrix Membranes

Freestanding asymmetric UiO-66-NH$_2$-PVA-PVAm MMM was obtained using a solution-casting method. For this purpose, the ratio of PVA: PVAm 4:1 wt.% from which 4 g of PVAm (5 wt.%) and 1 g of PVA (5 wt.%) were dissolved separately into the mixture of ethanol and water (30/70 v/v%) solvent and the solution was stirred overnight at room temperature. The desired amount of UiO-66-NH$_2$ particles were added into the PVA solution and maintained for the hydrothermal process at 110 °C for 24 h. The obtained vivid yellowish-green product was filtered and washed with ethanol and water two times and dried at room temperature. The obtained UiO-66-NH$_2$-PVA powder was added into the PVAm homogenous solution and left for overnight stirring at room temperature. The final solution was kept in a 20 min ultra-sonication-degassing mode for the degassing process and cast on a glassy plate using a micrometer regulating film applicator by adjusting the high on 300 μm to obtain ~40 μm average size of membrane thickness after evaporation of the solvents at vacuum oven at 80 °C for 24 h.

2.5. Gas Permeation Measurements

Similar to the previous report [18] the gas mixture permeation of the PVAm-PVA-UiO-66-NH$_2$ membranes was conducted using a gas permeation module connected to the gas chromatograph (TR-TC6891N). The CO$_2$/N$_2$ mixture as the feed side passed through a humidifier and a dehumidifier at room temperature and the sweep gas to saturate with water vapor. The gas flow feed rates were fixed as equimolar fractions of a binary mixture of CO$_2$ and N$_2$ (50 mL/min) to the permeation cell with the diameter of 42 mm. Reproduced membranes were tested, and the average steady-state values of the measurement results were reported with deviation. The permeability was expressed as Barrer (1 Barrer = 1×10^{-10} cm^3 (STP) cm/(cm^2 s cmHg) = 7.5005×10^{-18} m^2 s^{-1} Pa^{-1}) as follows:

$$P_i = (Q_i\ L)/(A\ \Delta p_i) \tag{1}$$

where Q_i is the volumetric flow rate of component i, L is the membrane thickness in (cm), A is the membrane area (cm^2), and Δp_i is the trans-membrane pressure difference of i component (in cmHg). The membrane thickness was measured using a bench micrometer and was double-checked with SEM cross-sectional observation. The separation factor α (A/B) for mixed-gas permeation was calculated by the following equation:

$$\alpha\ (A/B) = P_A/P_B \tag{2}$$

where P_A and P_B are the permeability of the gas components A and B of the permeate side.

3. Results and Discussions

3.1. Characterization of UiO-66-NH$_2$ and MMMs

To study the chemical structure and the MOF–polymer interactions, ATR–FTIR and analysis were employed (Figure 1). The main characteristic peaks of synthesized UiO-66-NH$_2$ were observed at 1575 cm^{-1} [ν(C=O)], 3349 cm^{-1} and 648 cm^{-1} [ν(N–H)], 648 cm^{-1} [ν(C=O)], 1383 cm^{-1} [ν(C–N)] [18]. The peaks located at 3349 cm^{-1} and 1575 cm^{-1} were assigned to the primary amines and the symmetric stretching vibration of carboxyl groups from 2-aminoterephtalic acid used for synthesis UiO-66-NH$_2$. The wide band observed in the PVA sample, between 3500–3000 cm^{-1}, referred to the stretching OH from intermolecular hydrogen bonds [20]. The vibration bands at 2898 cm^{-1} and 1730 cm^{-1} are assigned to the C–H from alkyl and acetate groups, respectively [21]. The large bands observed between 3200–2800 cm^{-1} and 1091 cm^{-1} were assigned to the primary and secondary existing amine groups in the PVAm sample. The observed amine groups in PVAm were connected to the hydroxyl group of PVA and afterward connected to the amines group of UiO-66-NH$_2$ through the intermolecular hydrogen bonds [22]. This resulted in the linkage of UiO-66-NH$_2$ to the PVAm matrix covalently, through the PVA. Created bridges via the covalent bonds between PVAm and UiO-66-NH$_2$ [18] are indicated

by the red-peak shift from 1575 cm^{-1} to 1641 cm^{-1} and the increased intensity of the secondary and primary amines groups (1077 cm^{-1} and 2388 cm^{-1}) in the MMM samples.
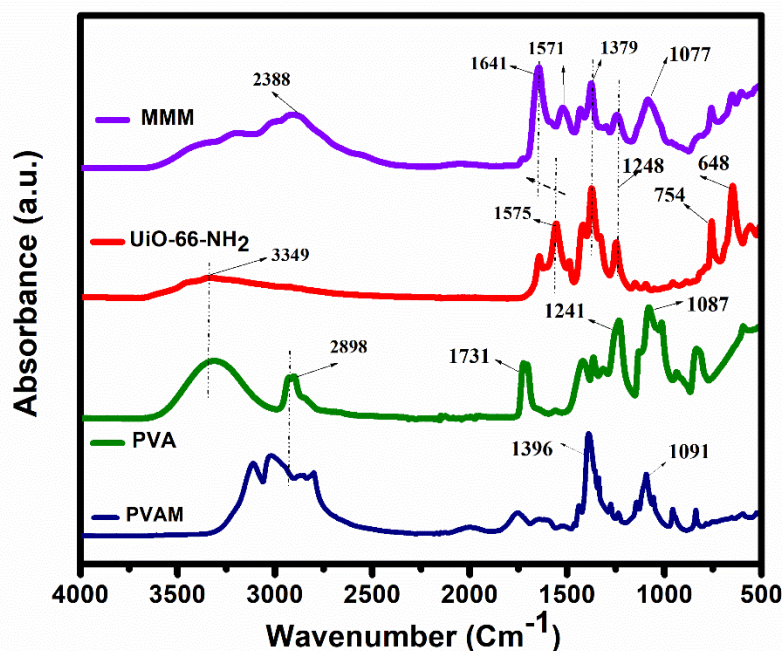

Figure 1. ATR–FTIR spectra of fabricated MMM and the synthesized UiO-66-NH$_2$ MOF.

The cross-sectional view of the PVAm membrane showed a typical asymmetric structure, with a dense selective layer and porous bulk morphology (Figure 2a,b) [23,24]. The UiO-66-NH$_2$ crystal structure exhibited triangular base pyramid morphology. The effect of poor and good MOF–polymer adhesion in the fabricated membranes is demonstrated in Figures 2 and 3. The significant phase separation domains between MOF and the polymer matrix and the agglomerated MOF regions were observed in the PVAm-UiO-66-NH$_2$ membrane (Figure 2d–g). While the homogenous MOF dispersion into the PVAm matrix was obtained using the PVA polymer chain, PVA was the connection bridge between UiO-66-NH$_2$ and PVA (Figure 3). SEM analysis and further SEM-EDS mapping (Figure 4) were also applied to study the cross-sectional morphology of the MMM and MOF particle distribution. As shown in Figure 3a, the MMM of PVAm-PVA-UiO-66-NH$_2$ with a thickness of ~70 μm was obtained. Unlike the PVAm-UiO-66-NH$_2$ sample (Figure 2f,g), the MOF particles were dispersed improperly, forming non-selective voids and cracks into the membrane matrix.

Adversely, owing to the high interaction and strong adhesion between PVA with the MOF and the polymer matrix, appropriate dispersion of UiO-66-NH$_2$ with almost no formation of sieve-in-a-cage morphology was observed (Figure 3c,d). Surface observation of the MMM in comparison with the PVAm-UiO-66-NH$_2$ shown the full coverage of the non-selective domains using the PVA bridging (Figure 3e,f). The observed hillock structure (Figure 3g) was attributed to the embedded MOF particles which truly demonstrated the interfacial compatibility with PVAm through the PVA bridges polymer segments.

Moreover, from Figure 3f, can be seen that the MOFs particles migrated to the surface of the membrane, which offers fast pathway channels for reactive gases with UiO-66-NH$_2$ such as CO$_2$. The XRD results confirmed this hypothesis since the crystallinity changed in the polymer matrix (Figure 5).
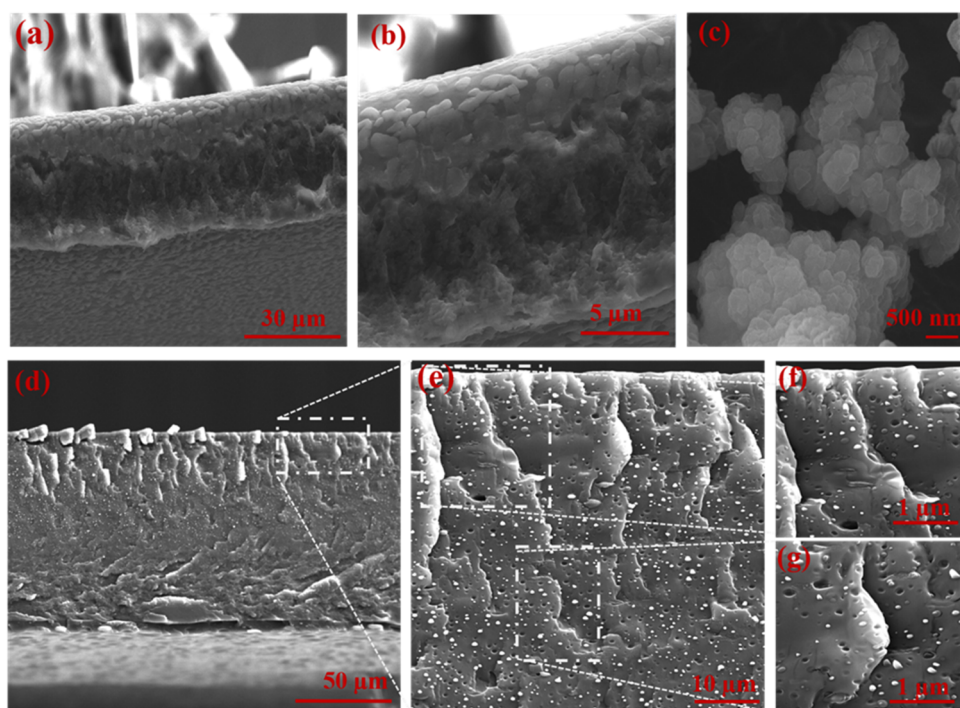
Figure 2. SEM images of cross-sectional view PVAm (**a**,**b**), UiO-66-NH$_2$ particles (**c**), and PVAm-UiO-66-NH$_2$ cross-sectional view (**d**–**g**).
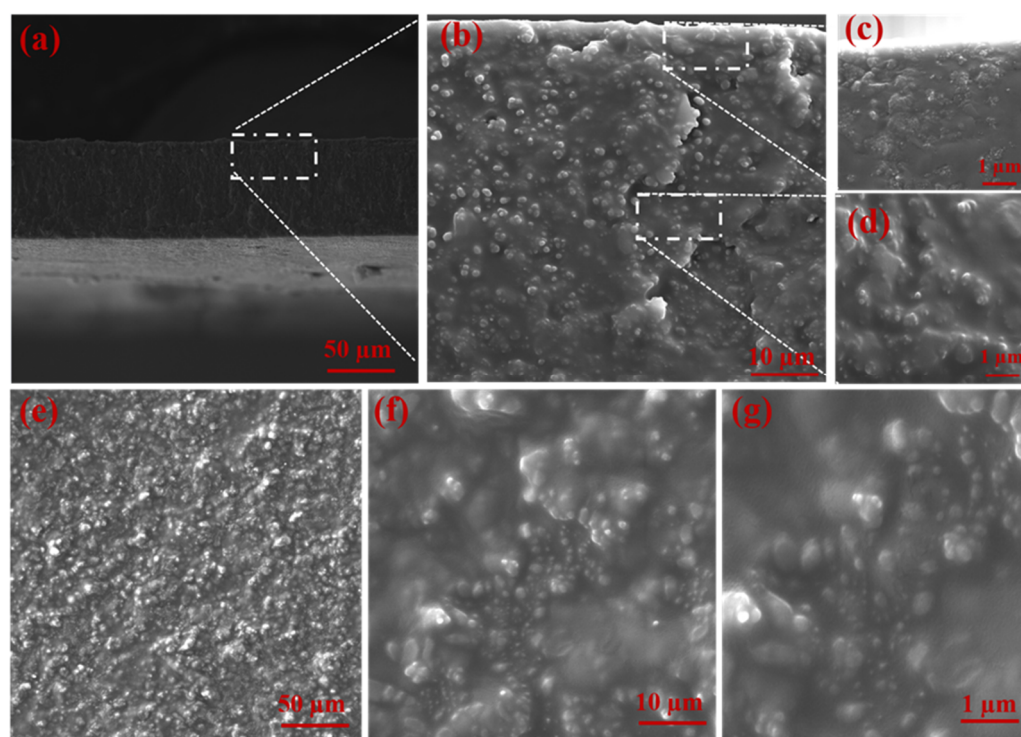
Figure 3. SEM images of cross-sectional view PVAm-PVA-UiO-66-NH$_2$ (**a**–**d**) and the surface morphology PVAm-PVA-UiO-66-NH$_2$ (**e**–**g**).
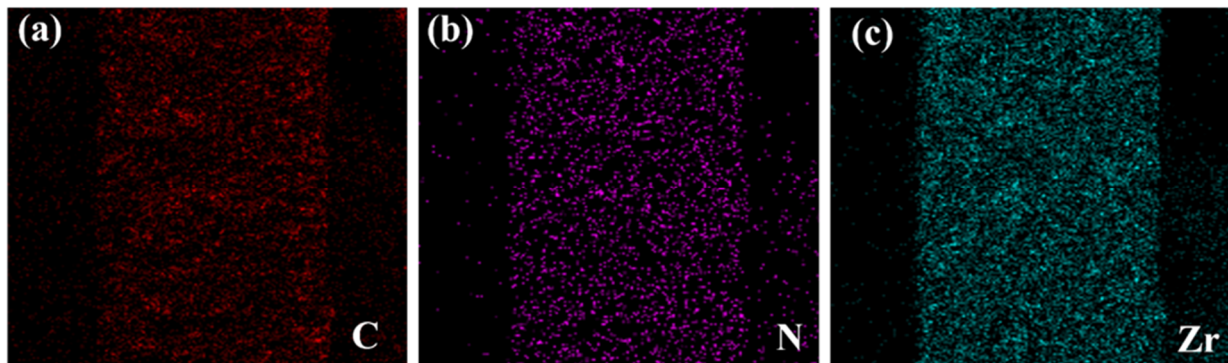
Figure 4. EDS of (**a**) C, (**b**) N, and (**c**) Zr elemental mapping of PVAm-PVA-UiO-66-NH$_2$.
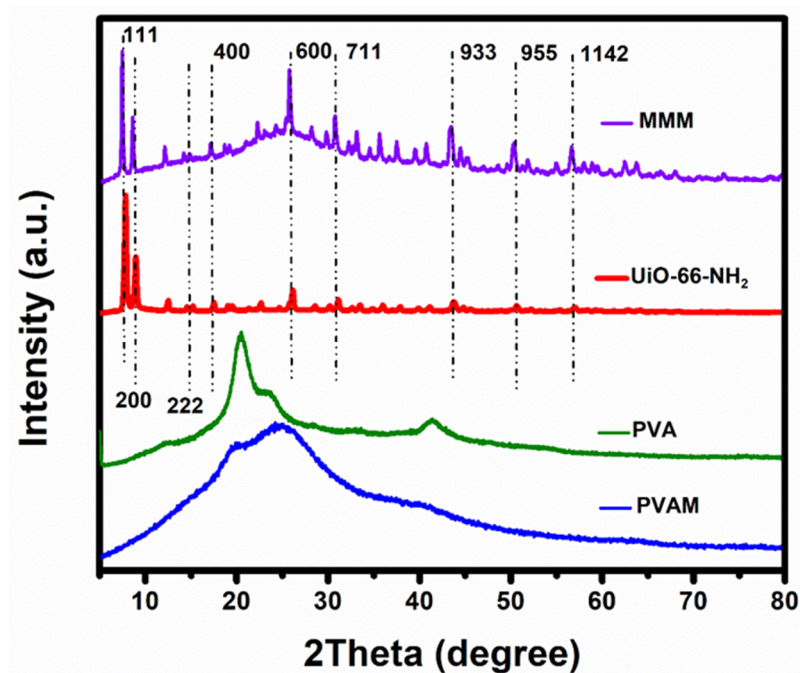

Figure 5. XRD spectra of fabricated MMM and the synthesized UiO-66-NH$_2$ MOF.

In other words, dispersion of MOFs particles refurbishes the polymeric membrane morphology and the crystalline lamellae domains. The MOF particle dispersion into a polymeric film was generally assumed to provide two main opposing effects, on one side increasing the free volume of the polymer, resulting in crystallinity decrement, and on the other side, effecting the polymer backbone-chain movement. Such a change in crystallinity leads to an increase in the polymer chain free volume. As shown in Figure 5, the three sharp peaks at 7.5°, 8.7°, and 26.7° in the XRD pattern for synthesized UiO-66-NH$_2$ and the fabricated MMM, compared to the PVA and PVAm pristine samples, showed good agreement with the those mentioned above [25]. The optical surface profiler of samples was depicted in Figure 6. It can be seen that the PVAm membrane surface showed the freckled structure (Figure 6a), while after incorporation of MOFs the domains of UiO-66-NH$_2$ were observed on the surface of the MMM. However, after using PVA as a bridges (Figure 6c) the membrane showed uniform dispersion of MOFs compared to the PVAm-UiO-66-NH$_2$ membrane (Figure 6b).
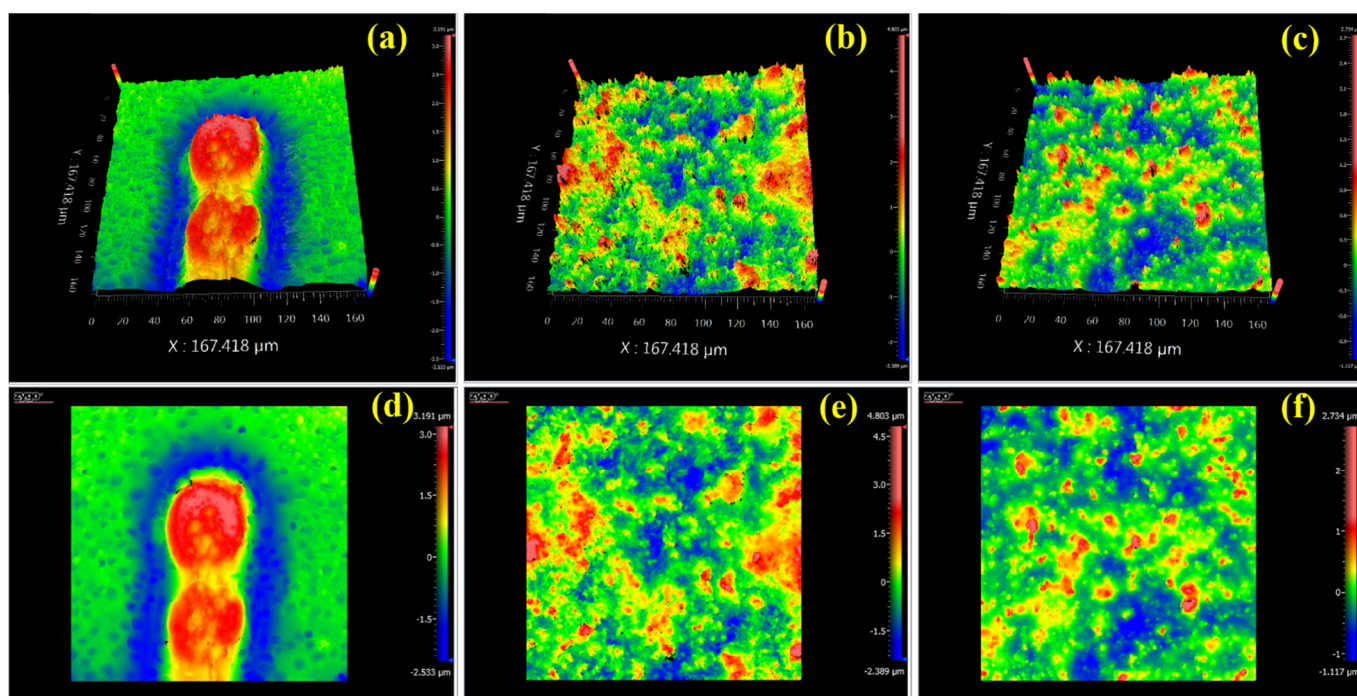
Figure 6. 3D and 2D Optical surface profiler of PVAm (**a**,**d**), PVAm-UiO-66-NH$_2$ (**b**,**e**) and PVAm-PVA-UiO-66-NH$_2$ (**c**,**f**).

3.2. Gas Permeation Performance of MMM

Sufficient amine functional groups provided from PVAm and UiO-66-NH$_2$ enabled the characteristics of facilitated transport mixed matrix membranes (FT-MMM) in humidified conditions. The main characteristic of FT-MMM is the reversible chemical reaction of CO$_2$ gas with complexing agents or carriers such as amine groups to transfer the reactive gases (e.g., CO$_2$). The presence of amino groups in the membrane also leads to the homogenous dispersion of MOF particles, by strengthening the MOF–polymer interface interactions, resulting in the nearly defect-free morphology of the MMM.

On one hand, it strengthens the polymer–particle interface interactions, leading to an improvement in the uniformity and adhesion of MOF particles distribution in the polymer matrix, leading to constructing a nearly defect-free interface. On the other hand, the fixed amino group sites provide CO$_2$ selective absorbability and desorbability via a reversible weak acid–base reaction resulting in high selectivity of CO$_2$ per nonreactive gases. Different amounts of UiO-66-NH$_2$ particles were dissolved with PVA followed by being incorporated into the PVAm matrix to conceive the effect of amino groups and MOFs loading effect on gas permeation. As shown in Figure 7, CO$_2$ permeability always increased by MOFs loading increments which is due to two main reasons.

Firstly, the porous structure of UiO-66-NH$_2$ provides accelerated transport channels for CO$_2$ to strengthen CO$_2$ permeability. Secondly, a sufficient primary amino group of MOFs reacting with CO$_2$ as a CO$_2$ carrier heightens the CO$_2$ permeability as was discussed before. Moreover, strong polymer–MOF affinity minimalized the interfacial defects in both the selective layer and bulk of the membrane. The compact and uniform dispersion of UiO-66-NH$_2$ nanoparticles on the membrane matrix offers continuous pathways for CO$_2$, while it hindered the non-reactive gas, N$_2$, from transferring. This led to the permeability privilege of CO$_2$ over N$_2$, which resulted in proper selectivity of CO$_2$/N$_2$ (Figure 8). The trend of the UiO-66-NH$_2$ loading effect on the trade-off manner of FT-MMM is illustrated in Figure 9. The trends in Figure 9 show the relationship between MOF loading, CO$_2$ permeability, and the CO$_2$/N$_2$ selectivity and also show the comparison of this work with the literature.
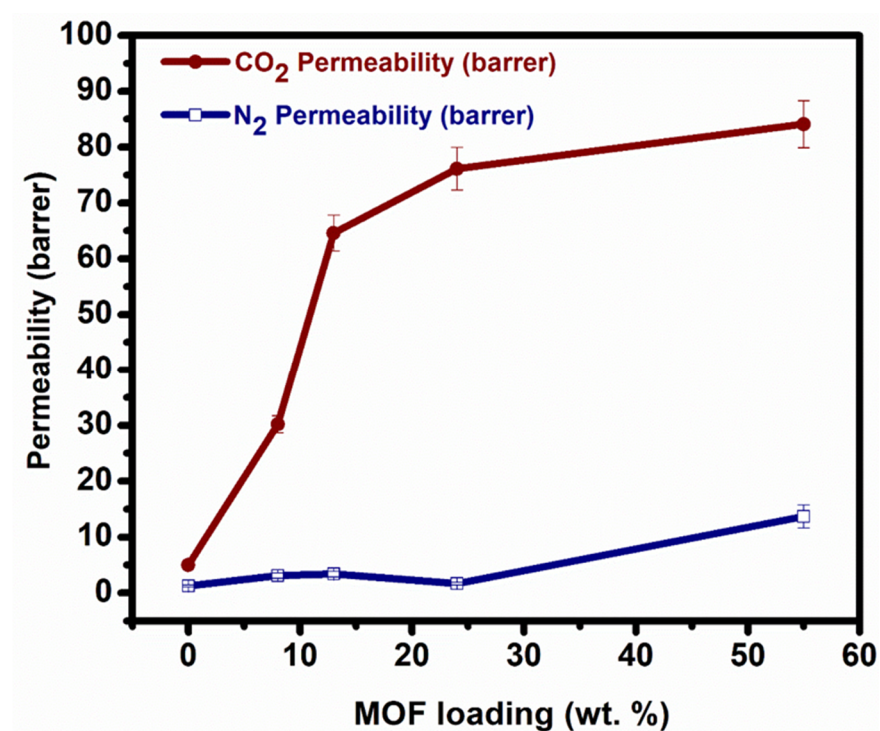
Figure 7. A dependence of CO_2 and N_2 gas permeability behavior of PVAm-PVA-UiO-66-NH$_2$ MMM with different UiO-66-NH$_2$ loading amounts.
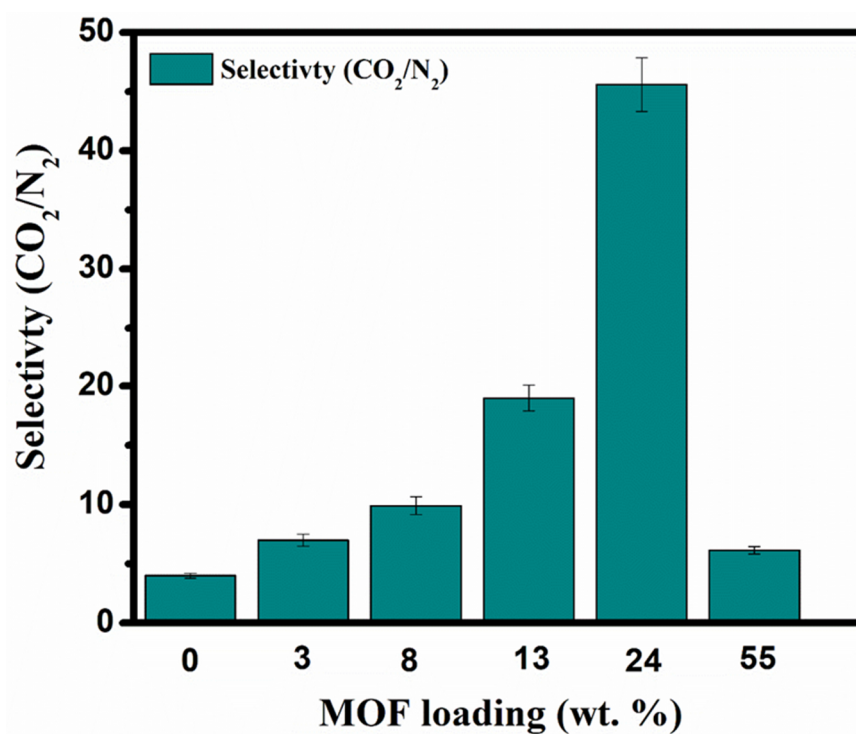

Figure 8. CO_2 and N_2 gas selectivity behavior of PVAm-PVA-UiO-66-NH$_2$ MMM with different UiO-66-NH$_2$ loading amounts.
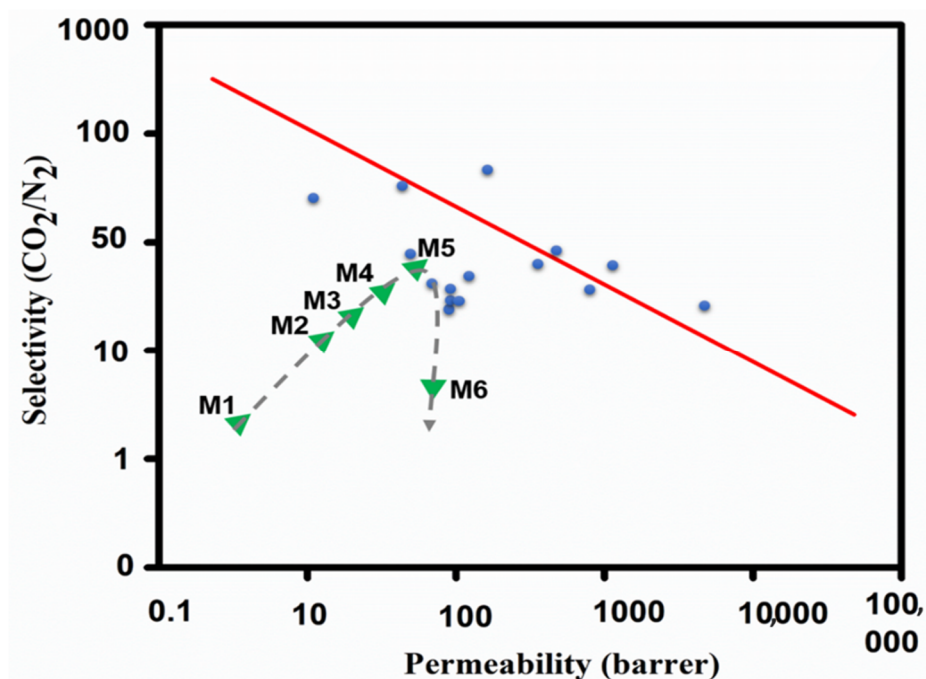
Figure 9. Robeson upper bound for CO_2/N_2 separations of M1–M6 membranes (0–55 wt.% of MOF loading). The 2008 upper bound line illustrates the tradeoff between permeability and selectivity, adapted from Refs. [9,26].

4. Conclusions

Our previous "bridging technique" was, in this work, successfully used for the UiO-66-NH_2 particles bonding with PVA, and afterward incorporated into the PVAm matrix. Such MOF loading to the PVAm matrix through the PVA bridges provided the opportunity for high MOF loading up to 55 wt.% incorporation of MOF amount into the PVAM matrix, without observing any sieve-in-a-cage morphology or unwanted cracks and voids. Furthermore, the sufficient amount of –NH_2 functional groups, provided by UiO-66-NH_2 and PVAm, provided fixed CO_2 carrier sites into the MMM to facilitate the preferential CO_2 permeation through the bicarbonate reversible reaction between CO_2 and –NH_2 in humidified conditions. However, the non-reactive gas such as N_2 could not easily pass through the MMM, neither by size exclusion nor solution-diffusion mechanism, due to the dense structure of the fabricated membranes as demonstrated in higher selectivity of CO_2 over N_2 gas molecules. The bridging technique offers a versatile and effective approach to fabricate almost defect-free MMM morphology with a high amount of MOFs loading for gas separation.

Author Contributions: S.A. and K.F. contributed equally to design, convinced, and wrote the draft of this work. C.R. conducted the analysis and M.K. improved the manuscript and helped analysis description. All authors have read and agreed to the published version of the manuscript.

Institutional Review Board Statement: Not applicable.

Informed Consent Statement: Not applicable.

Data Availability Statement: Not applicable.

Conflicts of Interest: The authors declare no conflict of interest. The funders had no role in the design of the study; in the collection, analyses, or interpretation of data; in the writing of the manuscript, or in the decision to publish the results.

References

1. Mason, C.R.; Maynard-Atem, L.; Heard, K.W.J.; Satilmis, B.; Budd, P.M.; Friess, K.; Lanč, M.; Bernardo, P.; Clarizia, G.; Jansen, J.C. Enhancement of CO2Affinity in a Polymer of Intrinsic Microporosity by Amine Modification. *Macromolecules* **2014**, *47*, 1021–1029. [CrossRef] [PubMed]
2. Wade, C.R.; Dincă, M. Investigation of the synthesis, activation, and isosteric heats of CO2 adsorption of the isostructural series of metal–organic frameworks M3(BTC)2 (M = Cr, Fe, Ni, Cu, Mo, Ru). *Dalton Trans.* **2012**, *41*, 7931–7938. [CrossRef] [PubMed]
3. Agrawal, R.; Rowles, H.C.; Kinard, G.E. *Cryogenics*; Wiley: Hoboken, NJ, USA, 2000.
4. Liu, S.; Shao, L.; Chua, M.L.; Lau, C.H.; Wang, H.; Quan, S. Recent progress in the design of advanced PEO-containing membranes for CO2 removal. *Prog. Polym. Sci.* **2013**, *38*, 1089–1120. [CrossRef]
5. Barelli, L.; Bidini, G.; Gallorini, F.; Servili, S. Hydrogen production through sorption-enhanced steam methane reforming and membrane technology: A review. *Energy* **2008**, *33*, 554–570. [CrossRef]
6. Vinoba, M.; Bhagiyalakshmi, M.; Alqaheem, Y.; Alomair, A.A.; Pérez, A.; Rana, M.S. Recent progress of fillers in mixed matrix membranes for CO 2 separation: A review. *Sep. Purif. Technol.* **2017**, *188*, 431–450. [CrossRef]
7. Bushell, A.F.; Attfield, M.P.; Mason, C.R.; Budd, P.M.; Yampolskii, Y.; Starannikova, L.; Rebrov, A.; Bazzarelli, F.; Bernardo, P.; Jansen, J.C.; et al. Gas permeation parameters of mixed matrix membranes based on the polymer of intrinsic microporosity PIM-1 and the zeolitic imidazolate framework ZIF-8. *J. Membr. Sci.* **2013**, *427*, 48–62. [CrossRef]
8. Boháčová, M.; Zetková, K.; Knotek, P.; Bouša, D.; Friess, K.; Číhal, P.; Lanč, M.; Hrdlička, Z.; Sofer, Z. Mildly oxidized SWCNT as new potential support membrane material for effective H2/CO2 separation. *Appl. Mater. Today* **2019**, *15*, 335–342. [CrossRef]
9. Robeson, L.M. The upper bound revisited. *J. Membr. Sci.* **2008**, *320*, 390–400. [CrossRef]
10. Galizia, M.; Chi, W.S.; Smith, Z.P.; Merkel, T.C.; Baker, R.W.; Freeman, B.D. 50th Anniversary Perspective: Polymers and Mixed Matrix Membranes for Gas and Vapor Separation: A Review and Prospective Opportunities. *Macromolecules* **2017**, *50*, 7809–7843. [CrossRef]
11. Sysel, P.; Minko, E.; Hauf, M.; Friess, K.; Hynek, V.; Vopička, O.; Pilnáček, K.; Šípek, M. Mixed matrix membranes based on hyperbranched polyimide and mesoporous silica for gas separation. *Desalin. Water Treat.* **2011**, *34*, 211–215. [CrossRef]
12. Ashtiani, S.; Khoshnamvand, M.; Shaliutina-Kolešová, A.; Bouša, D.; Sofer, Z.; Friess, K. Co0·5Ni0·5FeCrO4 spinel nanoparticles decorated with UiO-66-based metal-organic frameworks grafted onto GO and O-SWCNT for gas adsorption and water purification. *Chemosphere* **2020**, *255*, 126966. [CrossRef]
13. Furukawa, H.; Cordova, K.E.; O'Keeffe, M.; Yaghi, O.M. The Chemistry and Applications of Metal-Organic Frameworks. *Science* **2013**, *341*, 1230444. [CrossRef]
14. Wu, C.; Zhang, K.; Wang, H.; Fan, Y.; Zhang, S.; He, S.; Wang, F.; Tao, Y.; Zhao, X.; Zhang, Y.-B.; et al. Enhancing the Gas Separation Selectivity of Mixed-Matrix Membranes Using a Dual-Interfacial Engineering Approach. *J. Am. Chem. Soc.* **2020**, *142*, 18503–18512. [CrossRef]
15. Hossain, I.; Husna, A.; Chaemchuen, S.; Verpoort, F.; Kim, T.-H. Cross-Linked Mixed-Matrix Membranes Using Functionalized UiO-66-NH2 into PEG/PPG–PDMS-Based Rubbery Polymer for Efficient CO2 Separation. *ACS Appl. Mater. Interfaces* **2020**, *12*, 57916–57931. [CrossRef] [PubMed]
16. Kwon, H.T.; Jeong, H.-K. In Situ Synthesis of Thin Zeolitic–Imidazolate Framework ZIF-8 Membranes Exhibiting Exceptionally High Propylene/Propane Separation. *J. Am. Chem. Soc.* **2013**, *135*, 10763–10768. [CrossRef]
17. McDonald, K.A.; Feldblyum, J.I.; Koh, K.; Wong-Foy, A.G.; Matzger, A.J. Polymer@MOF@MOF: "grafting from" atom transfer radical polymerization for the synthesis of hybrid porous solids. *Chem. Commun.* **2015**, *51*, 11994–11996. [CrossRef]
18. Ashtiani, S.; Khoshnamvand, M.; Bouša, D.; Šturala, J.; Sofer, Z.; Shaliutina-Kolešová, A.; Gardenö, D.; Friess, K. Surface and interface engineering in CO2-philic based UiO-66-NH2-PEI mixed matrix membranes via covalently bridging PVP for effective hydrogen purification. *Int. J. Hydrogen Energy* **2021**, *46*, 5449–5458. [CrossRef]
19. Wu, H.; Li, X.; Li, Y.; Wang, S.; Guo, R.; Jiang, Z.; Wu, C.; Xin, Q.; Lu, X. Facilitated transport mixed matrix membranes incorporated with amine functionalized MCM-41 for enhanced gas separation properties. *J. Membr. Sci.* **2014**, *465*, 78–90. [CrossRef]
20. Mansur, H.S.; Sadahira, C.M.; Souza, A.N.; Mansur, A.A. FTIR spectroscopy characterization of poly (vinyl alcohol) hydrogel with different hydrolysis degree and chemically crosslinked with glutaraldehyde. *Mater. Sci. Eng. C* **2008**, *28*, 539–548. [CrossRef]
21. Andrade, G.I.; Barbosa-Stancioli, E.F.; Mansur, A.A.P.; Vasconcelos, W.L.; Mansur, H.S. Small-angle X-ray scattering and FTIR characterization of nanostructured poly (vinyl alcohol)/silicate hybrids for immunoassay applications. *J. Mater. Sci.* **2008**, *43*, 450–463. [CrossRef]
22. Deng, L.; Kim, T.-J.; Hägg, M.-B. Facilitated transport of CO2 in novel PVAm/PVA blend membrane. *J. Membr. Sci.* **2009**, *340*, 154–163. [CrossRef]
23. Pinnau, I.; Koros, W.J. A qualitative skin layer formation mechanism for membranes made by dry/wet phase inversion. *J. Polym. Sci. Part B Polym. Phys.* **1993**, *31*, 419–427. [CrossRef]

24. Ashtiani, S.; Khoshnamvand, M.; Číhal, P.; Dendisová, M.; Randová, A.; Bouša, D.; Shaliutina-Kolešová, A.; Sofer, Z.; Friess, K. Fabrication of a PVDF membrane with tailored morphology and properties via exploring and computing its ternary phase diagram for wastewater treatment and gas separation applications. *RSC Adv.* **2020**, *10*, 40373–40383. [CrossRef]

25. Qian, Q.; Wu, A.X.; Chi, W.S.; Asinger, P.A.; Lin, S.; Hypsher, A.; Smith, Z.P. Mixed-Matrix Membranes Formed from Imide-Functionalized UiO-66-NH2 for Improved Interfacial Compatibility. *ACS Appl. Mater. Interfaces* **2019**, *11*, 31257–31269. [CrossRef] [PubMed]

26. Han, Y.; Ho, W.W. Recent advances in polymeric membranes for CO2 capture. *Chin. J. Chem. Eng.* **2018**, *26*, 2238–2254. [CrossRef]